Published in final edited form as:
Mol Pharm. 2012 May 7; 9(5): 1441–1448. doi:10.1021/mp300019c.

Positron Emission Tomography Imaging of Tumor Angiogenesis with a ^{66}Ga-Labeled Monoclonal Antibody

Jonathan W. Engle[1,5], **Hao Hong**[2,5], **Yin Zhang**[1], **Hector F. Valdovinos**[1], **Duane V. Myklejord**[2], **Todd E. Barnhart**[1], **Charles P. Theuer**[3], **Robert J. Nickles**[1,*], and **Weibo Cai**[1,2,4,*]

[1]Department of Medical Physics, University of Wisconsin - Madison, WI, USA

[2]Department of Radiology, University of Wisconsin - Madison, WI, USA

[3]TRACON Pharmaceuticals, Inc., San Diego, CA, USA

[4]University of Wisconsin Carbone Cancer Center, Madison, WI, USA

Abstract

The goal of this study was to develop a ^{66}Ga-based positron emission tomography (PET) tracer for non-invasive imaging of CD105 expression during tumor angiogenesis, a hallmark of cancer. ^{66}Ga was produced using a cyclotron with ^{nat}Zn or isotopically enriched ^{66}Zn targets. TRC105, a chimeric anti-CD105 monoclonal antibody, was conjugated to 2-S-(4-isothiocyanatobenzyl)-1, 4, 7-triazacyclononane-1, 4, 7-triacetic acid (p-SCN-Bn-NOTA) and labeled with 66Ga. No difference in CD105 binding affinity or specificity was observed between TRC105 and NOTATRC105 based on flow cytometry analysis. Reactivity of ^{66}Ga for NOTA, corrected to the end of bombardment, was between 74 and 222 GBq/μmol for both target enrichments with < 2 ppb of cold gallium. ^{66}Ga-labeling was achieved with > 80% radiochemical yield. Serial PET imaging revealed that the murine breast cancer 4T1 tumor uptake of ^{66}Ga-NOTA-TRC105 was 5.9 ± 1.6, 8.5 ± 0.6, and 9.0 ± 0.6 %ID/g at 4, 20, and 36 h post-injection, respectively (n = 4). At the last time point, tumor uptake was higher than all organs which gave excellent tumor contrast with a tumor/muscle ratio of 10.1 ± 1.1. Biodistribution data as measured by gamma counting were consistent with the PET findings. Blocking experiment, control studies with ^{66}Ga-NOTA-cetuximab, as well as ex vivo histology all confirmed the in vivo target specificity of ^{66}Ga-NOTA-TRC105. Successful PET imaging with high specific activity ^{66}Ga (> 700 GBq/μmol has been achieved) as the radiolabel opens many new possibilities for future PET research with antibodies or other targeting ligands.

Keywords

^{66}Ga; Positron emission tomography (PET); Tumor angiogenesis; CD105/Endoglin; TRC105; Breast cancer

INTRODUCTION

The radionuclide ^{66}Ga ($t_{1/2}$ = 9.3 h, 56.5% β^+, 43.5% electron capture) is a useful surrogate for ^{67}Ga ($t_{1/2}$ = 78.3 h) and ^{68}Ga ($t_{1/2}$ = 68.3 min), which are used for single photon

[*]**Requests for reprints:** Weibo Cai, PhD, Departments of Radiology and Medical Physics, University of Wisconsin-Madison, Room 7137, 1111 Highland Avenue, Madison, WI 53705-2275, USA wcai@uwhealth.org; Phone: 608-262-1749; Fax: 608-265-0614 OR Robert J. Nickles, PhD, Department of Medical Physics, University of Wisconsin - Madison, Room B1305, 1111 Highland Avenue, Madison, WI 53705-2275, USA rnickles@wisc.edu; Phone: 608-263-1026 .
[5]Contributed equally to this work

emission computed tomography (SPECT) and positron emission tomography (PET) imaging, respectively.[1-3] Modern preclinical PET scanners capably cope with both fast positrons and prompt gamma emissions that are characteristic of many non-standard radionuclides, including ^{68}Ga and ^{66}Ga.[4, 5] The relatively long half-life of ^{66}Ga makes it a more practical radiolabel for peptides, proteins, and antibodies, whose slower in vivo kinetics are poorly matched by the much shorter half-life of ^{68}Ga.[6] Labeling chemistry with radiogallium has been well studied because of the popularity of ^{68}Ga from ^{68}Ge/^{68}Ga generators, as well as its production in very high specific activities relative to other radiometals (e.g. ^{64}Cu, ^{89}Zr, etc.).

Past work with ^{66}Ga has been limited, due to the relatively low specific activities achieved using previously reported methods, as well as the high energy gammas and positrons characteristic of its decay. Lewis *et al.* irradiated natural and enriched zinc targets to produce ^{66}Ga which was purified by cation exchange chromatography and solvent extraction, with the latter separation method been used in most ^{66}Ga-based studies to date.[7] However, the final reactivity of ^{66}Ga did not exceed 4.6 GBq/μmol of chelant, which was more than 100 fold below the theoretical limit. Subsequently, this method has been used to produce ^{66}Ga-DOTA-D-Phe^{1}-Tyr^{3}-octreotide[6] (DOTA denotes 1, 4, 7, 10-tetraazacyclododecane-1, 4, 7, 10-tetraacetic acid) and ^{66}Ga-deferoxamine-folate[8] for PET imaging applications, as well as to label chitosan complexes with ^{66}Ga for radiotherapy after intratumoral injection.[9] Direct production and separation of ^{66}Ga-citrate has been accomplished using anion exchange chromatography.[10] However, this strategy affords few prospects for radiolabeling of targeting ligands.

Recently, we have produced high specific activity ^{66}Ga from ^{nat}Zn(p,n) and ^{66}Zn(p,n) with a cyclotron using proton irradiations between 7 and 16 MeV,[11] which has resulted in specific activity of > 70 GBq/μmol for common bifunctional chelators, many fold higher that the reported literature values (< 4.6 GBq/μmol). In this study, we investigated the characteristics of ^{66}Ga-based immunoPET of tumor angiogenesis, a hallmark of solid tumor progression.[12] The protein target we have chosen for this study was CD105, also called “endoglin”, a 180 kDa disulphide-linked homodimeric transmembrane protein.[13-16] Considered as the “gold standard” marker of proliferating endothelium, CD105 modulates TGF-β receptor signaling through serine/threonine kinases, mainly modifying the phosphorylation of Smad proteins.[14]

Clinically, high CD105 expression on tumor vascular endothelial cells correlates with poor prognosis in more than 10 solid tumor types.[14, 15] To date, molecular imaging of CD105 expression has been understudied and most literature reports on CD105 imaging were based on labeling anti-CD105 antibodies.[17-24] TRC105, a human/murine chimeric IgG1 monoclonal antibody (mAb) which binds to both human and murine CD105 (with a dissociation constant of ~ 30 picomolar for human CD105 and within the nanomolar range for murine CD105), has been evaluated in a multicenter Phase 1 first-in-human dose-escalation trial in the United States.[25] Multiple Phase 2 clinical trials are underway in patients with various solid tumor types (e.g. breast, prostate, bladder, ovarian, and liver cancer). In this work, we conjugated TRC105 with NOTA (1, 4, 7-triazacyclononane-1, 4, 7-triacetic acid) for ^{66}Ga-labeling and investigated ^{66}Ga-NOTA-TRC105 for immunoPET of CD105 expression during tumor angiogenesis in a murine breast cancer model.

EXPERIMENTAL SECTION

Reagents

^{nat}Zn foils (0.25 mm thick) and $^{nat}ZnCl_2$, both of 99.999% purity, were purchased from Sigma Aldrich (St. Louis, MO). Isotopically enriched ^{66}Zn (98.58%) was acquired from

Isoflex (San Francisco). TRC105 was provided by TRACON Pharmaceuticals, Inc. (San Diego, CA). Cetuximab (a human/murine chimeric IgG1 mAb that binds to human epidermal growth factor receptor [EGFR] but does not cross-react with murine EGFR[26]) was from Bristol-Myers Squibb Company (Princeton, NJ). AlexaFluor488- and Cy3-labeled secondary antibodies were purchased from Jackson Immunoresearch Laboratories, Inc. (West Grove, CA). 2-S-(4-isothiocyanatobenzyl)-1, 4, 7-triazacyclononane-1, 4, 7-triacetic acid (abbreviated as p-SCN-Bn-NOTA) and Chelex 100 resin (50-100 mesh) were purchased from Macrocyclics, Inc. (Dallas, TX) and Sigma-Aldrich, respectively. Cation exchange resin (AG50W-X4, 100-200 mesh) was acquired from Bio-Rad (Hercules, CA). Trace-metals grade HCl was purchased from VWR (Radnor, PA). Water and all buffers were of Millipore grade and pre-treated with Chelex 100 resin to ensure that the aqueous solution was heavy metal-free. PD-10 desalting columns were purchased from GE Healthcare (Piscataway, NJ). All other chemicals were purchased from Thermo Fisher Scientific (Fair Lawn, NJ).

Cell Lines and Animal Model

4T1 murine breast cancer, MCF-7 human breast cancer, and human umbilical vein endothelial cells (HUVECs) were purchased from the American Type Culture Collection (ATCC, Manassas, VA). Cells were cultured as described previously and used for in vitro and in vivo experiments when they reached ~80% confluence.[23] All animal studies were conducted under a protocol approved by the University of Wisconsin Institutional Animal Care and Use Committee. The 4T1 tumor model was established as previously described and mice were used for in vivo experiments when the diameter of tumors reached 5-8 mm (typically 1-2 weeks after inoculation).[23]

Production of ^{66}Ga

Targets of ^{nat}Zn or ^{66}Zn were electrodeposited from 0.05 N hydrochloric acid solution onto gold or silver target backings with dimensions matched to the cyclotron beam of a General Electric (Waukesha, WI) PETtrace cyclotron.[11] Targets were irradiated with 20 - 30 μA of 13 MeV protons for between 1 and 3 h, dissolved in concentrated HCl, and purified by cation exchange chromatography with successive additions of 10 N and 7 N HCl to recover the Zn target material and elute trace contaminant metals. The product was collected in 4 N HCl, evaporated to dryness, and redissolved in 0.1 N HCl prior to buffering. If the target of ^{nat}Zn was used, ^{68}Ga was allowed to decay overnight before target processing commenced. In this case, the only radioisotopic contaminant was ^{67}Ga, present as < 5% of the radioactivity at 16 h after the end of bombardment (EoB). On the other hand, radioisotopic purity of ^{66}Ga produced from the ^{66}Zn target exceeded 99.9%.

NOTA Conjugation and ^{66}Ga-Labeling

NOTA conjugation to mAbs (TRC105 and cetuximab) was carried out as previously described.[27, 28] Briefly, TRC105 or cetuximab was mixed with p-SCN-Bn-NOTA at pH 9.0 with a molar ratio of 1:25 and the resulting NOTA-TRC105 or NOTA-cetuximab was purified with size exclusion chromatography. For radiolabeling, 74-111 MBq of ^{66}Ga-acetate (pH 5.5) was prepared from 0.1 N HCl solution by addition of 0.25 M NH_4OAc solution (pH 7.2), which was then added to a solution of NOTA-TRC105 or NOTA-cetuximab with 25 μg of NOTA-mAb conjugate per 37 MBq of ^{66}Ga. The reaction mixture was incubated for 30 min at 37 °C with constant shaking. ^{66}Ga-NOTA-TRC105 and ^{66}Ga-NOTA-cetuximab were purified by size exclusion chromatography using normal saline buffered with 0.25 M NH_4OAc (pH 7.2) as the mobile phase. The radioactive fractions containing ^{66}Ga-NOTATRC105 or ^{66}Ga-NOTA-cetuximab were collected and passed through a 0.2 μm syringe filter prior to injection into tumor-bearing mice.

Flow Cytometry

The immunoreactivity of TRC105 and NOTA-TRC105 to HUVECs (high CD105 expression[20, 29]) and MCF-7 cells (CD105-negative[20]) were evaluated by fluorescence-activated cell sorting (FACS) analysis, as described previously.[20, 30] FACS studies were carried out using a BD FACSCalibur 4-color analysis cytometer (Becton-Dickinson, San Jose, CA), which is equipped with 488nm and 633nm lasers and FlowJo analysis software (Tree Star, Inc., Ashland, OR).

Imaging and Biodistribution Studies

PET and CT (with a voxel size of 210×210×210 μm^3) scans at various time points post-injection (p.i.) were performed using an Inveon microPET/microCT rodent model scanner (Siemens Medical Solutions USA, Inc.) as described previously,[23, 30] with a 2.8 nanosecond coincidence time window. The images were reconstructed using a maximum a posteriori (MAP) algorithm, with no attenuation or scatter correction. For each PET scan, three-dimensional regions-of-interest (ROIs) were drawn over the 4T1 tumor and major organs with vendor software (Inveon Research Workplace [IRW]) on decay-corrected whole-body images. Assuming a tissue density of 1 g/mL, the ROIs were converted to MBq/g using a conversion factor pre-determined using a 20 mL centrifuge tube filled with ~20 MBq of $^{66}GaCl_3$ as a phantom, and divided by the total administered radioactivity to obtain an image ROI-derived percentage injected dose per gram of tissue (%ID/g).

Four additional 4T1 tumor-bearing mice were each injected with 2 mg of unlabeled TRC105 at 2 h before ^{66}Ga-NOTA-TRC105 administration to evaluate the CD105 specificity of ^{66}Ga-NOTA-TRC105 in vivo (i.e. blocking experiment). Biodistribution studies were carried out to validate quantitative tracer uptake values derived from ROI analysis of PET scans against radioactivity distribution measured ex vivo. At 36 h p.i., mice were euthanized and blood, 4T1 tumor, and major organs/tissues were collected and wet-weighed. The radioactivity in each tissue was measured using a gamma-counter (Perkin Elmer) and presented as %ID/g (mean ± SD). The 4T1 tumor, liver, and spleen (i.e. tissues with significant uptake of ^{66}Ga-NOTA-TRC105) were also frozen for histological analysis.

Dose-Escalation Study

The effect of NOTA-TRC105 dose on the biodistribution of ^{66}Ga-NOTA-TRC105 in 4T1 tumor-bearing mice was investigated. Four groups of mice (three mice per group) each received ~4 MBq of ^{66}Ga-NOTA-TRC105, which contained escalating NOTATRC105 doses of 0.5, 5, 25, and 100 μg, respectively. At 36 hours p.i., mice were euthanized for biodistribution studies as described above.

Histology

Frozen tissue slices of 5 μm thickness were fixed with cold acetone for 10 min and dried in the air for 30 min. After rinsing with phosphate-buffered saline and blocking with 10% donkey serum for 30 min at room temperature, the slices were incubated with TRC105 (2 μg/mL) for 1 h at 4 °C and visualized using AlexaFluor488-labeled goat anti-human IgG. The tissue slices were also stained for endothelial marker CD31 as described previously.[31, 32] All images were acquired with a Nikon Eclipse Ti microscope.

Statistical Analysis

Quantitative data were expressed as mean ± SD. Means were compared using Student's t-test. P values < 0.05 were considered statistically significant.

RESULTS

Flow Cytometry Analysis

Based on FACS analysis of HUVECs which express high level of CD105, there was no observable difference between TRC105 and NOTA-TRC105 at 1 μg/mL or 5 μg/mL concentrations (Figure 1). The binding to HUVECs was antigen specific, as neither TRC105 nor NOTA-TRC105 bound to CD105-negative MCF-7 cells, even at a much higher concentration of 15 μg/mL (Figure 1). Taken together, FACS analysis indicated that NOTA conjugation did not alter the antigen binding affinity or specificity of TRC105.

^{66}Ga Production and Radiolabeling

Specific activity of ^{66}Ga for NOTA, measured by titration with various concentrations of NOTA and corrected to EoB, was between 74 and 222 GBq/μmol for both target enrichments. Inductively coupled plasma mass spectrometry (ICP-MS) detected < 2 ppb of cold gallium and < 20 ppb of iron in the final ^{66}Ga solutions. ^{66}Ga-labeling, including purification using PD-10 columns, took 70 ± 10 min (n = 7). The decay-corrected radiochemical yield was 80.2 ± 4.1 %, based on 25 μg of antibody conjugate (NOTA-TRC105 or NOTA-cetuximab) per 37 MBq of ^{66}Ga, with radiochemical purity of > 95%. The ratio of ^{66}Ga activity to antibody mass was ~1.2 GBq/mg of antibody for both ^{66}Ga-NOTA-TRC105 and ^{66}Ga-NOTA-cetuximab, assuming complete recovery of the NOTA-mAb conjugates after size exclusion chromatography.

Small Animal PET Imaging

Based on the half-life of ^{66}Ga (9.3 h), 4, 20, and 36 h p.i. were chosen as the time points for serial PET scans after intravenous tracer injection. The coronal slices that contained the 4T1 tumors are shown in Figure 2A and representative PET/CT fused images of a mouse at 20 h p.i. of ^{66}Ga-NOTA-TRC105 are shown in Figure 2B. The quantitative data obtained from ROI analysis are shown in Figure 3. Because of the superb stability of the ^{66}Ga-NOTA complex, liver uptake of ^{66}Ga-NOTA-TRC105 in 4T1 tumor-bearing mice was significantly lower at all time points examined than that observed for ^{64}Cu-DOTA-TRC105 in our previous study (> 25.0 %ID/g at 4 h p.i, which may reflect a certain degree of ^{64}Cutranschelation hence elevated liver uptake of radioactivity).[20] Meanwhile, blood pool activity was prominent at early time points (due to long circulation half-life of the antibody conjugate) and gradually declined thereafter. The liver uptake of ^{66}Ga-NOTA-TRC105 was 10.6 ± 1.8, 8.2 ± 0.4, and 6.8 ± 0.5 %ID/g at 4, 20, and 36 h p.i. respectively, whereas the radioactivity in the blood was 10.3 ± 1.9, 9.4 ± 0.9, and 9.0 ± 0.6 %ID/g at 4, 20, and 36 h p.i. respectively (n = 4; Figure 3A). Importantly, tumor uptake of ^{66}Ga-NOTA-TRC105 was clearly visible as early as 4 h p.i. and plateaued at around 20 h p.i. (5.9 ± 1.6, 8.5 ± 0.6, and 9.0 ± 0.6 %ID/g at 4, 20, and 36 h p.i. respectively; n = 4; Figure 3A&D).

Administration of a blocking dose of TRC105 at 2 h before ^{66}Ga-NOTA-TRC105 injection reduced the tumor uptake to 4.4 ± 1.2, 5.8 ± 0.6, and 7.2 ± 0.6 %ID/g at 4, 20, and 36 h p.i. respectively (n = 4; Figure 2A, 3B&D). Statistically significant differences were achieved at 20 and 36 h p.i. ($P < 0.05$) when compared with the tumor uptake in mice injected with ^{66}Ga-NOTA-TRC105 alone, which indicated CD105 specificity of the tracer in vivo. Liver uptake of ^{66}Ga-NOTA-TRC105 in the blocking group (11.2 ± 2.0, 7.2 ± 0.8, and 5.3 ± 0.7 %ID/g at 4, 20, and 36 h p.i. respectively; n = 4) was comparable to that of mice injected with ^{66}Ga-NOTATRC105 alone. A similar trend was also observed for radioactivity in the blood (11.8 ± 1.6, 9.4 ± 0.9, and 8.0 ± 0.9 %ID/g at 4, 20, and 36 h p.i. respectively for the blocking group; n = 4; Figure3B). Overall, tracer uptake in all major organs was similar between the two groups yet the 4T1 tumor uptake was significantly higher in mice injected

with ^{66}Ga-NOTA-TRC105 alone than in the blocking group, confirming CD105 specificity of the tracer in vivo.

To further investigate CD105 specificity of ^{66}Ga-NOTA-TRC105, ^{66}Ga-NOTA-cetuximab was used as an isotype-matched control. Both TRC105 and cetuximab are human/murine chimeric IgG1 mAbs. Since cetuximab does not cross-react with murine tissues, it serves as a suitable control for evaluating tracer uptake in the tumor due to passive targeting alone (i.e. the enhanced permeability and retention [EPR] effect[33]). As can be seen in Figure 2A, 3C&D, 4T1 tumor uptake of ^{66}Ga-NOTA-cetuximab was 2.7 ± 0.5, 4.2 ± 1.2, and 4.1 ± 0.8 %ID/g at 4, 20, and 36 h p.i. respectively (n = 4), significantly lower than that of ^{66}Ga-NOTA-TRC105 at all time points examined ($P < 0.05$ at 4 h p.i. and $P < 0.01$ at 20 and 36 h p.i.) and confirmed CD105 specificity of ^{66}Ga-NOTA-TRC105 in vivo.

Biodistribution Studies

All mice were euthanized after the last PET scans at 36 h p.i. for biodistribution studies to validate the in vivo PET data. Besides the 4T1 tumor, blood also had significant radioactivity at 36 h p.i., which was expected for a radiolabeled antibody (Figure 4A). When compared with all major organs in mice, the uptake of ^{66}Ga-NOTA-TRC105 in the 4T1 tumor was higher, which provided good tumor contrast with a tumor/muscle ratio of 10.1 ± 1.1 at 36 h p.i. (n = 4). Pre-injection of a blocking dose of TRC105 led to a significant decrease in 4T1 tumor uptake ($P < 0.01$; n = 4; Figure 4A) with similar uptake in the blood and liver, corroborating PET results.

A comparison of the biodistribution data between the two tracers at 36 h p.i. revealed that the uptake of ^{66}Ga-NOTA-cetuximab was similar to ^{66}Ga-NOTA-TRC105 in most organs except the 4T1 tumor and blood (Figure 4B), which again indicated specific tumor targeting of ^{66}Ga-NOTA-TRC105 ($P < 0.01$ when comparing the 4T1 tumor uptake between the two tracers). Dose-escalation study revealed that there was no significant difference in the 4T1 tumor uptake of ^{66}Ga-NOTA-TRC105, at doses ranging from 0.5 μg to 100 μg of NOTA-TRC105 per mouse (Figure 5). At 36 h p.i., tracer uptake in the 4T1 tumor was 8.8 ± 1.2, 9.9 ± 1.2, 8.5 ± 0.5, and 8.0 ± 0.5 %ID/g for 0.5, 5, 25, and 100 μg of NOTA-TRC105 per mouse, respectively. Overall, quantitative data from ex vivo biodistribution studies and in vivo PET scans were in good agreement, confirming that ROI analysis of non-invasive PET scans accurately reflected tracer distribution in vivo.

Histology

Immunofluorescence staining revealed that CD105 expression in the 4T1 tumor was primarily located on the tumor vasculature, as evidenced by excellent co-localization of CD105 and CD31 staining (Figure 6). Since tumor vasculature is generally more actively proliferating in the peripheral region than in the center of the tumor, uptake of ^{66}Ga-NOTA-TRC105 in the 4T1 tumor was rather heterogeneous (i.e. higher uptake in the peripheral region and lower uptake in the tumor center).

CD105 staining of mouse liver and spleen both gave very low signal, indicating that these tissues do not express CD105. Therefore, uptake of ^{66}Ga-NOTA-TRC105 in the liver/spleen was largely unrelated to CD105 binding and more likely attributed to non-specific capture by the reticuloendothelial system and hepatic clearance of the antibody-based tracer. Taken together, histological findings corroborated the in vivo data of ^{66}Ga-NOTA-TRC105, warranting further investigation and application of this tracer.

DISCUSSION

PET has been widely used in clinical oncology for cancer staging and monitoring the therapeutic response.[34-37] The goal of this study was to evaluate the in vivo performance of ^{66}Ga-NOTATRC105 for PET imaging of tumor angiogenesis. ^{66}Ga is suited for this purpose since its decay characteristics matches the in vivo kinetics of the labeled mAb. In addition, the stability of NOTA as a chelator for radiogallium has been well documented in the literature.[1] As confirmed by the in vivo study, the stability of ^{66}Ga-NOTA-TRC105 (indicated by blood radioactivity and liver capture) was clearly higher than that previously reported for ^{64}Cu-DOTA-TRC105.[20]

Although ^{66}Ga has higher positron energy (E_{max} of 4.15 MeV) than other commonly used PET isotopes (e.g. E_{max} of 1.90 MeV for ^{68}Ga), high energy positrons (which can lead to a longer positron range) and co-emitted gammas (which can affect image reconstruction and quantitation) have only a small effect on the PET image quality and quantitation accuracy (Figure 2, 4), further enabling researchers to consider future use of the versatile radiometal for PET. It was reported that for glass capillaries using filtered back projection, the full widths at half maximum for ^{68}Ga PET using the Inveon microPET scanner was 2.46 mm (which had a mean positron range of 3.48 mm in water), while the full widths at half maximum for ^{18}F PET was 1.81 mm (which had a mean positron range of 0.62 mm in water).[38] To ensure that the quantitative results obtained from ROI analysis of the PET scans in our study were accurate, a solution of ^{66}Ga with known amount of radioactivity was used as the phantom to correlate PET measurement to the true radioactivity concentration.

^{66}Zn is a more economical cyclotron target than the feedstocks used to produce other radiometals commonly used for PET applications (e.g. ^{64}Ni for ^{64}Cu), and we have produced ^{66}Ga with reactivities for DOTA and NOTA approaching 740 GBq/μmol (i.e. 20 Ci/μmol) using ^{66}Zn targets. ^{68}Ga has been used to label a wide variety of compounds, which sets the stage for future investigation of these compounds with the longer-lived ^{66}Ga. For example, many tracers (some are currently in clinical investigation) can only be imaged with PET within a few hours after injection, due to the short 68.3 min half-life of ^{68}Ga. The use of ^{66}Ga can allow for PET imaging at later time points to evaluate the long term fate of these tracers, which may provide more biological insights. Besides the significantly higher specific activity of ^{66}Ga than many other radiometals such as ^{89}Zr, the high energy positron emission (although not ideal for PET imaging) also makes ^{66}Ga a desirable isotope for Cerenkov luminescence imaging, a research topic that is under active investigation.[39, 40]

Compared with other PET tracers (e.g. peptide-based),[41-43] labeled antibodies are desirable agents for imaging of tumor angiogenesis due to their high affinity for the targets and long circulation half-lives, as the target mass is usually low (only a few percentage of the total tumor mass). One major challenge in radiolabeling of antibodies is the minimization of interference with their antigen binding affinity and specificity. The complementarity-determining region (CDR) of TRC105 each contains only one lysine residue,[16] among a total of ~1400 amino acid residues and ~70 lysines in the whole antibody. Therefore, the possibility of NOTA conjugation at the lysine residue within the CDR is extremely low. Indeed, FACS analysis confirmed that NOTA-TRC105 maintained high avidity to its target at several non-antigen-saturating conditions (Figure 1) and did not bind to CD105-negative cells. Based on the specific activity of ^{66}Ga, it was calculated that there were 0.8 ~ 2.4 ^{66}Ga per TRC105.

The imaging target of our study, CD105, is primarily present on the tumor neovasculature. Even though the 4T1 tumor cells are CD105-negative per se (the fluorescence signal for CD105 staining of the tumor is predominantly on the tumor vasculature but not on the 4T1

cells; Figure 6), they grow rapidly when inoculated into mice and contain a highly angiogenic tumor vasculature with prominent CD105 expression, which allowed for noninvasive PET imaging. The lack of CD105 expression on the tumor cells is one reason why uptake of ^{66}Ga-NOTA-TRC105 in the 4T1 tumor is not as high as that observed for certain other antibody-based tracers,[32, 44] which target tumor cells rather than the tumor vasculature. In solid tumors, typically there are significantly fewer tumor vascular endothelial cells than tumor cells.

Partly due to the excellent stability of the ^{66}Ga-NOTA complex, blood radioactivity of ^{66}Ga-NOTA-TRC105 was prominent even at late time points (~10 %ID/g at 20 and 36 h p.i.), which could lead to appreciable tumor uptake attributed to the EPR effect.[33] Therefore, both the ^{66}Ga-NOTA-TRC105 and the blocking group exhibited an increasing trend of tumor uptake over time. In future studies, radiolabeled antibody fragments of TRC105 (e.g. F(ab')$_2$) may exhibit less EPR effect-based tumor uptake and give better tumor/blood ratio. ^{66}Ga-NOTA-cetuximab had significantly lower blood radioactivity level at late time points (~5%ID/g), which resulted in lower tumor uptake based on the EPR effect alone, as well as the absence of an increasing trend in the tumor uptake level. The blood radioactivity difference of isotype-matched IgG1 mAbs (e.g. TRC105 and cetuximab) may be attributed to many factors, including antigen binding or lack thereof, different interactions with the neonatal Fc receptor (FcRn) which binds to the CH_2-CH_3 hinge regions in the constant region (Fc) of IgG antibodies (notably the amino acid sequences in the Fc region may be different even for isotype-matched antibodies),[45, 46] variable glycosylation patterns in the Fc regions, etc.

CONCLUSION

We report the use of ^{66}Ga as a radiolabel for immunoPET imaging of CD105, a protein overexpressed on actively proliferating tumor endothelial cells. CD105-specific tumor targeting was achieved with ^{66}Ga-NOTA-TRC105, which also exhibited appreciable tumor uptake attributed to the EPR effect. Successful PET imaging with ^{66}Ga as the radiolabel, which can be produced with high reactivities (up to 740 GBq/μmol for NOTA), opens many possibilities for more detailed clinical/preclinical investigations of a wide variety of PET agents that were previously limited by the short half-life of ^{68}Ga. In addition, the suitable half-life also makes ^{66}Ga a desirable isotope for immunoPET, which has been a vibrant research field over the last several decades.

Acknowledgments

This work is supported, in part, by the University of Wisconsin Carbone Cancer Center, the Department of Defense (W81XWH-11-1-0644), the National Center for Advancing Translational Sciences (NCATS) grant 9U54TR000021, the Elsa U. Pardee Foundation, and the NIH through the UW Radiological Sciences Training Program 5 T32 CA009206-32.

REFERENCES

(1). Velikyan I. Positron emitting ^{68}Ga-based imaging agents: chemistry and diversity. Med. Chem. 2011; 7:345–79. [PubMed: 21711223]

(2). Even-Sapir E, Israel O. Gallium-67 scintigraphy: a cornerstone in functional imaging of lymphoma. Eur. J. Nucl. Med. Mol. Imaging. 2003; 30(Suppl 1):S65–81. [PubMed: 12644887]

(3). Severin GW, Knutson LD, Voytas PA, George EA. Half-life of ^{66}Ga. Phys. Rev. C. 2010; 82:067301.

(4). Laforest R, Rowland DJ, Welch MJ. MicroPET imaging with nonconventional isotopes. IEEE Trans. Nucl. Sci. 2002; 49:2119–2126.

(5). Graham MC, Pentlow KS, MAwlawi O, Finn RD, Daghighian F, Larson SM. An investigationof the physical characteristics of ^{66}Ga an an isotope for PET imaging and quantification. Med. Phys. 1997; 24:317–327. [PubMed: 9048374]

(6). Ugur O, Kothari PJ, Finn RD, Zanzonico P, Ruan S, Guenther I, Maecke HR, Larson SM. Ga-66 labeled somatostatin analogue DOTA-DPhe1-Tyr3-octreotide as a potential agent for positron emission tomography imaging and receptor mediated internal radiotherapy of somatostatin receptor positive tumors. Nucl. Med. Biol. 2002; 29:147–57. [PubMed: 11823119]

(7). Lewis MR, Reichert DE, Laforest R, Margenau WH, Shefer RE, Klinkowstein RE, Hughey BJ, Welch MJ. Production and purification of gallium-66 for preparation of tumor-targeting radiopharmaceuticals. Nucl. Med. Biol. 2002; 29:701–6. [PubMed: 12234596]

(8). Mathias CJ, Lewis MR, Reichert DE, Laforest R, Sharp TL, Lewis JS, Yang Z-F, Waters DJ, Snyder PW, Low PS, Welch MJ, Green MA. Preparation of ^{66}Ga- and ^{68}Ga-labeled Ga(III)-deferoxamine-folate as potential folate-receptor-targeted PET radiopharmaceuticals. Nucl. Med. Biol. 2003; 30:725–731. [PubMed: 14499330]

(9). Akhlaghi M, Pourjavadi A. Preparation and primary evaluation of ^{66}Ga-DTPA-chitosan in fibrosarcoma bearing mice. Nuckleonika. 2011; 56:41–47.

(10). El-Azony KM, Ferieg K, Saleh ZA. Direct separation of ^{67}Ga citrate from zinc and copper target materials by anion exchange. Appl. Radiat. Isot. 2003; 59:329–331. [PubMed: 14622930]

(11). Engle JW, Lopez-Rodriguez V, Gaspar-Carcamo RE, Valdovinos HF, Valle-Gonzalez M, Trejo-Ballado F, Severin GW, Barnhart TE, Nickles RJ, Avila-Rodriguez MA. Very high specific activity $^{66/68}$Ga from zinc targets for PET. Appl. Radiat. Isot. 2012 in press.

(12). Hanahan D, Weinberg RA. Hallmarks of cancer: the next generation. Cell. 2011; 144:646–74. [PubMed: 21376230]

(13). Fonsatti E, Altomonte M, Nicotra MR, Natali PG, Maio M. Endoglin (CD105): a powerful therapeutic target on tumor-associated angiogenetic blood vessels. Oncogene. 2003; 22:6557–63. [PubMed: 14528280]

(14). Dallas NA, Samuel S, Xia L, Fan F, Gray MJ, Lim SJ, Ellis LM. Endoglin (CD105): a marker of tumor vasculature and potential target for therapy. Clin. Cancer Res. 2008; 14:1931–7. [PubMed: 18381930]

(15). Fonsatti E, Nicolay HJ, Altomonte M, Covre A, Maio M. Targeting cancer vasculature via endoglin/CD105: a novel antibody-based diagnostic and therapeutic strategy in solid tumours. Cardiovasc. Res. 2010; 86:12–9. [PubMed: 19812043]

(16). Seon BK, Haba A, Matsuno F, Takahashi N, Tsujie M, She X, Harada N, Uneda S, Tsujie T, Toi H, Tsai H, Haruta Y. Endoglin-targeted cancer therapy. Curr. Drug Deliv. 2011; 8:135–43. [PubMed: 21034418]

(17). Bredow S, Lewin M, Hofmann B, Marecos E, Weissleder R. Imaging of tumour neovasculature by targeting the TGF-beta binding receptor endoglin. Eur. J. Cancer. 2000; 36:675–81. [PubMed: 10738134]

(18). Fonsatti E, Jekunen AP, Kairemo KJ, Coral S, Snellman M, Nicotra MR, Natali PG, Altomonte M, Maio M. Endoglin is a suitable target for efficient imaging of solid tumors: *in vivo* evidence in a canine mammary carcinoma model. Clin. Cancer Res. 2000; 6:2037–43. [PubMed: 10815930]

(19). Korpanty G, Carbon JG, Grayburn PA, Fleming JB, Brekken RA. Monitoring response to anticancer therapy by targeting microbubbles to tumor vasculature. Clin. Cancer Res. 2007; 13:323–30. [PubMed: 17200371]

(20). Hong H, Yang Y, Zhang Y, Engle JW, Barnhart TE, Nickles RJ, Leigh BR, Cai W. Positron emission tomography imaging of CD105 expression during tumor angiogenesis. Eur. J. Nucl. Med. Mol. Imaging. 2011; 38:1335–43. [PubMed: 21373764]

(21). Zhang Y, Hong H, Cai W. PET tracers based on Zirconium-89. Curr. Radiopharm. 2011; 4:131–139. [PubMed: 22191652]

(22). Yang Y, Zhang Y, Hong H, Liu G, Leigh BR, Cai W. In vivo near-infrared fluorescence imaging of CD105 expression. Eur. J. Nucl. Med. Mol. Imaging. 2011; 38:2066–76. [PubMed: 21814852]

(23). Hong H, Severin GW, Yang Y, Engle JW, Zhang Y, Barnhart TE, Liu G, Leigh BR, Nickles RJ, Cai W. Positron emission tomography imaging of CD105 expression with ^{89}Zr-Df-TRC105. Eur. J. Nucl. Med. Mol. Imaging. 2012; 39:138–148. [PubMed: 21909753]

(24). Deshpande N, Ren Y, Foygel K, Rosenberg J, Willmann JK. Tumor Angiogenic Marker Expression Levels during Tumor Growth: Longitudinal Assessment with Molecularly Targeted Microbubbles and US Imaging. Radiology. 2011; 258:804–11. [PubMed: 21339349]

(25). Mendelson DS, Gordon MS, Rosen LS, Hurwitz H, Wong MK, Adams BJ, Alvarez D, Seon BK, Theuer CP, Leigh BR. Phase I study of TRC105 (anti-CD105 [endoglin] antibody) therapy in patients with advanced refractory cancer. J. Clin. Oncol. 2010; 28:15s.

(26). Goldberg RM. Cetuximab. Nat. Rev. Drug Discov. 2005; (Suppl):S10–1. [PubMed: 15962524]

(27). Zhang Y, Hong H, Engle JW, Bean J, Yang Y, Leigh BR, Barnhart TE, Cai W. Positron Emission Tomography Imaging of CD105 Expression with a ^{64}Cu-Labeled Monoclonal Antibody: NOTA Is Superior to DOTA. PLoS One. 2011; 6:e28005. [PubMed: 22174762]

(28). Zhang Y, Hong H, Engle JW, Yang Y, Barnhart TE, Cai W. Positron emission tomography and near-infrared fluorescence imaging of vascular endothelial growth factor with dual-labeled bevacizumab. Am. J. Nucl. Med. Mol. Imaging. 2012; 2:1–13. [PubMed: 22229128]

(29). Takahashi N, Haba A, Matsuno F, Seon BK. Antiangiogenic therapy of established tumors in human skin/severe combined immunodeficiency mouse chimeras by anti-endoglin (CD105) monoclonal antibodies, and synergy between anti-endoglin antibody and cyclophosphamide. Cancer Res. 2001; 61:7846–54. [PubMed: 11691802]

(30). Zhang Y, Hong H, Engle JW, Yang Y, Theuer CP, Barnhart TE, Cai W. Positron Emission Tomography and Optical Imaging of Tumor CD105 Expression with a Dual-Labeled Monoclonal Antibody. Mol. Pharm. 2012; 9:645–53. [PubMed: 22292418]

(31). Cai W, Chen K, Mohamedali KA, Cao Q, Gambhir SS, Rosenblum MG, Chen X. PET of vascular endothelial growth factor receptor expression. J. Nucl. Med. 2006; 47:2048–2056. [PubMed: 17138749]

(32). Cai W, Wu Y, Chen K, Cao Q, Tice DA, Chen X. *In vitro* and *in vivo* characterization of ^{64}Cu-labeled Abegrin^{TM}, a humanized monoclonal antibody against integrin $\alpha_v\beta_3$. Cancer Res. 2006; 66:9673–81. [PubMed: 17018625]

(33). Maeda H, Wu J, Sawa T, Matsumura Y, Hori K. Tumor vascular permeability and the EPR effect in macromolecular therapeutics. A review. J. Control. Release. 2000; 65:271–84.

(34). Gambhir SS, Czernin J, Schwimmer J, Silverman DH, Coleman RE, Phelps ME. A tabulated summary of the FDG PET literature. J. Nucl. Med. 2001; 42:1S–93S. [PubMed: 11483694]

(35). Eary JF, Hawkins DS, Rodler ET, Conrad EUI. ^{18}F-FDG PET in sarcoma treatment response imaging. Am. J. Nucl. Med. Mol. Imaging. 2011; 1:47–53.

(36). Vach W, Høilund-Carlsen PF, Fischer BM, Gerke O, Weber W. How to study optimal timing of PET/CT for monitoring of cancer treatment. Am. J. Nucl. Med. Mol. Imaging. 2011; 1:54–62.

(37). Grassi I, Nanni C, Allegri V, Morigi JJ, Montini GC, Castellucci P, Fanti S. The clinical use of PET with ^{11}C-acetate. Am. J. Nucl. Med. Mol. Imaging. 2012; 2:33–47.

(38). Disselhorst JA, Brom M, Laverman P, Slump CH, Boerman OC, Oyen WJ, Gotthardt M, Visser EP. Image-quality assessment for several positron emitters using the NEMA NU 4-2008 standards in the Siemens Inveon small-animal PET scanner. J. Nucl. Med. 2010; 51:610–7. [PubMed: 20237025]

(39). Ruggiero A, Holland JP, Lewis JS, Grimm J. Cerenkov luminescence imaging of medical isotopes. J. Nucl. Med. 2010; 51:1123–30. [PubMed: 20554722]

(40). Thorek DLJ, Robertson R, Bacchus WA, Hahn J, Rothberg J, Beattie BJ, Grimm J. Cerenkov imaging - a new modality for molecular imaging. Am. J. Nucl. Med. Mol. Imaging. 2012; 2:163–173.

(41). Alauddin MM. Positron emission tomography (PET) imaging with ^{18}F-based radiotracers. Am. J. Nucl. Med. Mol. Imaging. 2012; 2:55–76.

(42). Hao G, Hajibeigi A, De León-Rodríguez LM, Öz OK, Sun X. Peptoid-based PET imaging of vascular endothelial growth factor receptor (VEGFR) expression. Am. J. Nucl. Med. Mol. Imaging. 2011; 1:65–75.

(43). Wang RE, Niu Y, Wu H, Amin MN, Cai J. Development of NGR peptide-based agents for tumor imaging. Am. J. Nucl. Med. Mol. Imaging. 2011; 1:36–46.

(44). Cai W, Ebrahimnejad A, Chen K, Cao Q, Li ZB, Tice DA, Chen X. Quantitative radioimmunoPET imaging of EphA2 in tumor-bearing mice. Eur. J. Nucl. Med. Mol. Imaging. 2007; 34:2024–36. [PubMed: 17673999]

(45). Roopenian DC, Akilesh S. FcRn: the neonatal Fc receptor comes of age. Nat. Rev. Immunol. 2007; 7:715–25. [PubMed: 17703228]

(46). Jefferis R, Lefranc MP. Human immunoglobulin allotypes: possible implications for immunogenicity. MAbs. 2009; 1:332–8. [PubMed: 20073133]

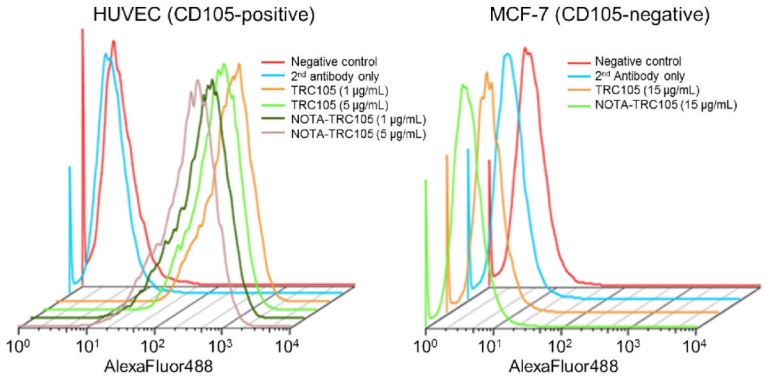

Figure 1.
Flow cytometry analysis of TRC105 and NOTA-TRC105 in HUVECs (CD105-positive) and MCF-7 cells (CD105-negative) at several non-antigen-saturating concentrations.

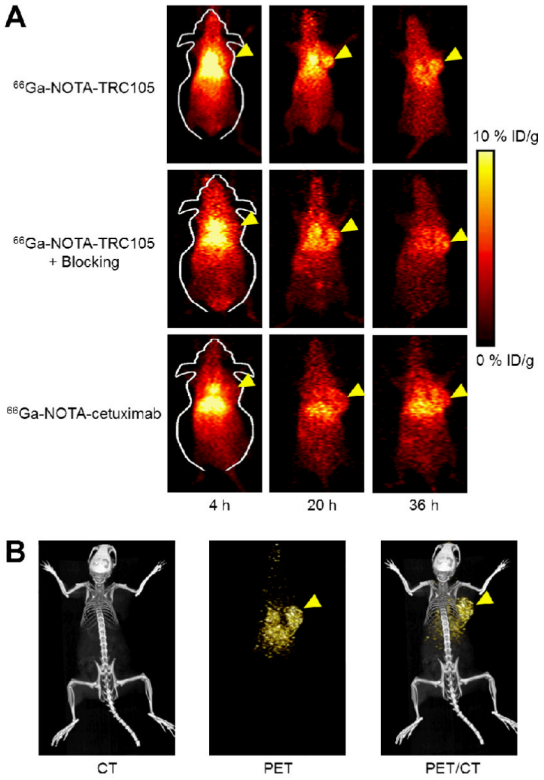

Figure 2.

Serial PET imaging of 4T1 tumor-bearing mice. (A) Coronal PET images at 4, 20, and 36 h post-injection of ^{66}Ga-NOTA-TRC105, 2 mg of TRC105 before ^{66}Ga-NOTA-TRC105 (i.e. blocking), or ^{66}Ga-NOTA-cetuximab. (B) Representative PET/CT images of ^{66}Ga-NOTATRC105 in 4T1 tumor-bearing mice at 20 h post-injection. Tumors are indicated by arrowheads.

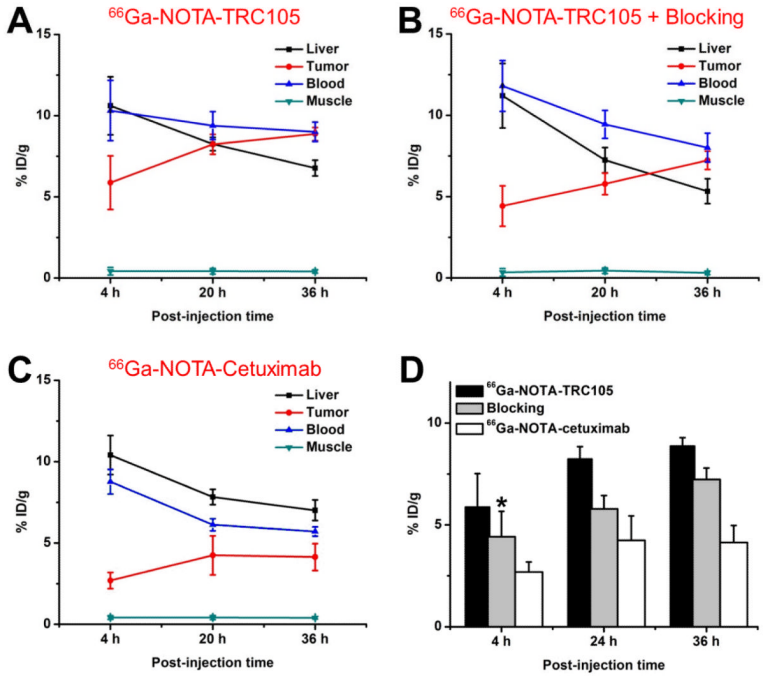

Figure 3.

Quantitative analysis of the PET data. (A) Time-activity curves of the liver, tumor, blood, and muscle upon intravenous injection of ^{66}Ga-NOTA-TRC105 into 4T1 tumor-bearing mice (n = 4). (B) Time-activity curves of the liver, tumor, blood, and muscle upon intravenous injection of ^{66}Ga-NOTA-TRC105, after a blocking dose of TRC105, into 4T1 tumor-bearing mice (n = 4). (C) Time-activity curves of the liver, tumor, blood, and muscle upon intravenous injection of ^{66}Ga-NOTA-cetuximab into 4T1 tumor-bearing mice (n = 4). (D) Comparison of tracer uptake in the 4T1 tumor among the three groups. P values are < 0.05 or < 0.01 in all cases when compared with the ^{66}Ga-NOTA-TRC105 group, except one case where P > 0.05 (denoted with "*").

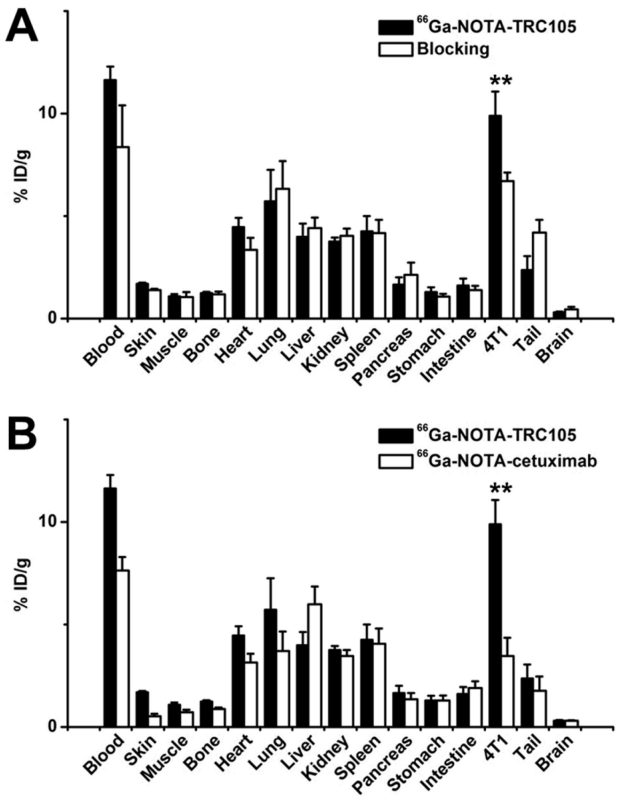

Figure 4.

Biodistribution studies in 4T1 tumor-bearing mice. (A) Biodistribution of ^{66}Ga-NOTATRC105 at 36 h post-injection, with or without a pre-injected blocking dose of TRC105 (n = 4). (B) Biodistribution of ^{66}Ga-NOTA-TRC105 and ^{66}Ga-NOTA-cetuximab at 36 h post-injection (n = 4). **: $P < 0.01$.

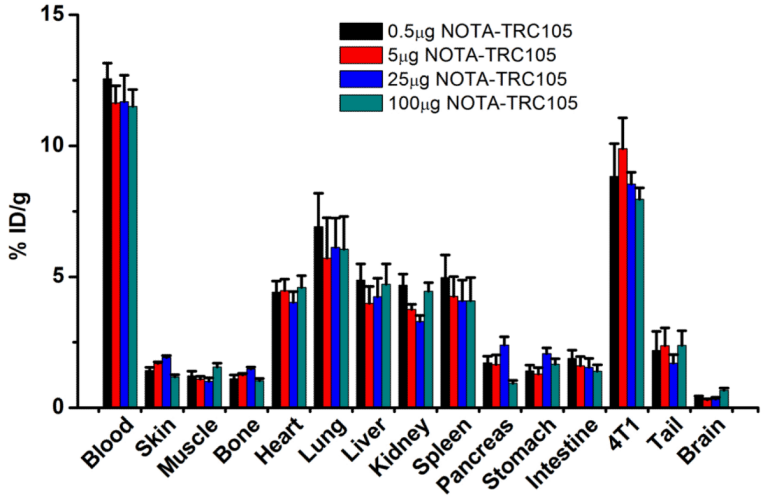

Figure 5.
The effect of NOTA-TRC105 dose on the biodistribution of ^{66}Ga-NOTA-TRC105 in 4T1 tumor-bearing mice (n = 3 per group).

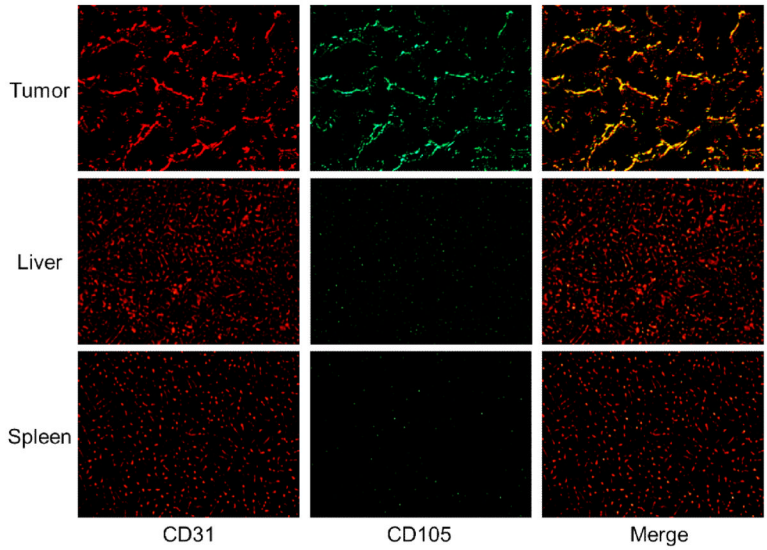

Figure 6.
Immunofluorescence CD105/CD31 staining of the 4T1 tumor, liver, and spleen tissue sections. CD31 staining was shown in red and CD105 staining was displayed in green. All images were acquired under the same condition and displayed at the same scale. Magnification: 200×.